

High intrinsic ZT in InP_3 monolayer at room temperature

Shenghui Zhang,^{1,2} Xiaobin Niu,² Yiqun Xie,^{1,*} Kui Gong,³ Hezhu Shao,^{4,†} Yibin Hu,^{5,‡} and Yin Wang⁶

¹Department of Physics, Shanghai Normal University, 100 Guilin Road, Shanghai 200232, P.R. China

²School of Materials and Energy, University of Electronic Science and Technology of China, Chengdu 610054, P.R. China

³Hongzhiwei Technology (Shanghai) CO.LTD., 1888 Xinqiniao Road, Pudong, Shanghai 201206, P.R. China

⁴Ningbo Institute of Materials Technology and Engineering,
Chinese Academy of Sciences, Ningbo 315201, P.R. China

⁵State Key Laboratory of Infrared Physics, Shanghai Institute of Technical Physics,
Chinese Academy of Sciences, Shanghai 200083, P.R. China

⁶Department of Physics and International Centre for Quantum and Molecular Structures,
Shanghai University, 99 Shangda Road, Shanghai 200444, P.R. China

Two-dimensional thermoelectric materials with a figure of merit ZT , which is greater than 2.0 at room temperature, would be highly desirable in energy conversion since the efficiency is competitive to conventional energy conversion techniques. Here, we propose that the indium triphosphide (InP_3) monolayer offers an extraordinary ZT of 2.2 at 300 K by using quantum calculations within the ballistic thermal transport region. A remarkably low and isotropic phononic thermal conductivity is founded, which is due to flat lattice vibration modes. This low thermal conductivity takes a major responsibility to the impressively high ZT . Moreover, a large ZT that is greater than 1.5 can be maintained, even if a 1% mechanic extension is applied on the lattice. These results suggest that the InP_3 monolayer is a promising candidate for low dimensional thermoelectric applications.

I. INTRODUCTION

Thermoelectric (TE) materials can realise direct energy conversion between heat and electricity, and have many potential applications in power generation and heat pumping¹. The efficiency of thermoelectric materials is determined by the dimensionless figure of merit, $ZT = \frac{\sigma S^2 T}{\kappa_e + \kappa_p}$, where σ is the electric conductivity, S is the seebeck coefficient, T is the absolute temperature and $\kappa_{p(e)}$ is the phononic (electronic) thermal conductivity². Great efforts have been put into finding thermoelectric materials with high ZT value. So far, a maximum ZT of 2.6 is reported in single crystal SnSe ³, and the ZT value increases to 2.8 in n-type SnSe crystal⁴. Whereas at the nanoscale, quantum confinement can substantially reduce the phononic thermal conductivity, thus lead to a considerable enhancement of the thermoelectric efficiency in nanostructures. There are great interests in thermoelectric properties of the low-dimensional materials since the ground-breaking experiments which indicate that rough silicon nanowire can be an efficient thermoelectric material⁵.

Currently, there are intense focus on the thermoelectricity of the 2D materials, such as the graphenene, silicene, black phosphorus and transition-metal dichalcogenides, due to their attractive electronic properties and thermal transport properties^{6–12}. For example, a theoretical calculation has shown that the ZT of silicene nanoribbon is close to 2.5 at 90 K.⁹ A large ZT of 2.8 at 800 K has been predicted for the monolayer SnSe .¹³ Such excellent thermoelectric performances of 2D materials, however, were obtained when the temperatures were far away from the room temperature.

In reality, 2D thermoelectric materials with a high ZT at room temperature will largely facilitate their utilizations, such as cooling and electricity generation. Un-

fortunately, the thermoelectric efficiency in the pristine 2D materials at room temperature is relatively poor, as the ZT is typically less than 2.0. For instance, the ZT of graphene is close to 0.01¹⁴, and those of the 2D black phosphorene and blue phosphorene are about 0.2 and 1.0, respectively.⁸ Moreover, 2D MX_2 ($M = \text{Mo}, \text{W}$; $X = \text{S}, \text{Se}$) monolayers have $ZT < 2$ at 300 K as predicated by theoretical calculation.⁷ So far, for the pristine 2D materials, the highest ZT at room temperature is 2.15, which is calculated for the monolayer buckled antimonene¹⁵.

There are several methods that can be used to improve the thermoelectric efficiency in 2D materials, including defects and strain engineering, chemical doping and heterostucure¹⁶. For instance, the ZT of graphene can be improved impressively to around 3.2 at room temperature using a layered structure with the phonon blocking materials¹⁷. Besides, the ZT of the antimonene can be largely improved from less than 0.1 to about 0.6 at room temperature by n -type doping¹⁸. Even though, new 2D materials with a better thermoelectric efficiency at room temperature are still highly desirable in order to facilitate their real applications.

In this work, we investigated the thermoelectric properties of the InP_3 monolayer, a newly predicted 2D material with remarkable electronic properties¹⁹, by using density functional theory combined with the non-equilibrium Green's functional formalisms (NEGF-DFT)²⁰. We obtained a large ZT of 2.2 at 300 K, due to the low thermal conductivity.

II. MODEL AND METHODS

The primitive cell of the InP_3 monolayer is presented in Figs. 1(a,b), which is composed of two In atoms and six P atoms bonded via covalent interactions with a hexag-

onal structure, similar to the silicene. The lattice constant of the InP₃ monolayer is 7.55Å optimized by VASP code²¹, which is consistent with the previous theoretical calculation¹⁹. Using this primitive cell, we calculated both the electronic and thermal transport properties of the InP₃ monolayer, and then obtained its thermoelectric properties. The details of the simulation methods are described in the following.

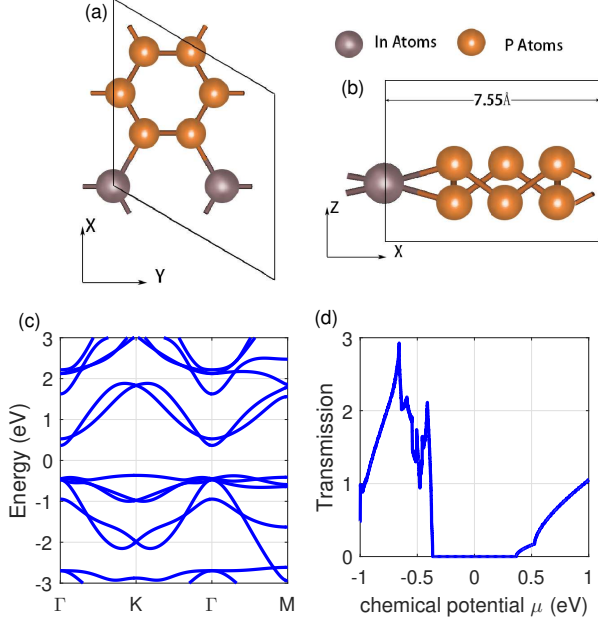


FIG. 1: Top (a) and side (b) views of the primitive cell of the InP₃ monolayer. Gray and yellow spheres denote the In and P atoms, respectively. The electronic bandstructure (c) and electronic transmission spectrum (d) of the InP₃ monolayer.

We optimize the lattice constant and obtain a force-constant calculated by VASP code²¹, and construct the dynamic matrix for the phonon spectrum calculation. During the optimization, the atoms are fully relaxed until the maximum force is less than 0.005 eV/Å. The plane wave was used for wave function expansion with a cutoff energy of 400 eV. The projector augmented-wave method²² was used for describing core electron. The PW91 version of the generalized gradient approximation (GGA) was used for the electron exchange and correlation functional²³. In structure relaxing, a $9 \times 9 \times 1$ k sampling was used. For calculating force-constant, a $3 \times 3 \times 1$ supercell was used, and k sampling reduced to $3 \times 3 \times 1$. Both the electronic and thermal transport properties were carried out using Nanocal code²⁴ within a NEGF-DFT theoretical method. In the calculation, $150 \times 150 \times 1$ k points were adopted. A double-zeta polarized (DZP) atomic orbital basis was used to expand all physical quantities, the exchanges and correlation was treated at the level of a generalized gradient approximation, and the atomic cores were defined using the standard norm-conserving nonlocal pseudopotentials. These calculation details were verified to provide accurate re-

sults.

Within the linear response limit, the electrical current and electrical thermal current can be defined by

$$I = \frac{2e}{h} \int T_e(E)(f_L(E) - f_R(E))dE \quad (1)$$

$$I_Q = \frac{2}{h} \int T_e(E)(f_L(E) - f_R(E))(E - \mu)dE \quad (2)$$

Here $T_e(\varepsilon)$ is the electronic transmission function, which can be calculated by the standard nonequilibrium Green's function method, and $f(\varepsilon, \mu) = 1/\{\exp[(\varepsilon - \mu)/k_B T] + 1\}$ is the Fermi-Dirac distribution function at the chemical potential μ .

For ballistic electronic transport, electronic transmission function can be calculated as

$$T_e(E) = \text{Tr}(G_e^r \Gamma_L G_e^a \Gamma_R) \quad (3)$$

$$\Gamma_L = i(\Sigma_L^r - \Sigma_L^a), \Gamma_R = i(\Sigma_R^r - \Sigma_R^a) \quad (4)$$

$$G_e^r = [ES - H - \Sigma_L^r - \Sigma_R^r]^{-1} \quad (5)$$

Here, G_e^r is retarded Green's function, H and S is hamiltonian and overlap matrix, Σ_L^r and Σ_R^r are self-energy from left and right semi-infinite leads.

From above equations, we can obtain electronic conductivity σ , Seebeck coefficient S and thermal conductivity κ_e ^{2,25}

$$\sigma = e^2 L_0 / l \quad (6)$$

$$S = -\frac{L_1}{eTL_0} \quad (7)$$

$$\kappa_e(T) = \frac{1}{Tl} \left(L_2 - \frac{L_1^2}{L_0} \right) \quad (8)$$

where l is the device length, and $L_m(\mu)$ is given by

$$L_m(\mu) = \frac{2}{h} \int_{-\infty}^{\infty} d\varepsilon T_e(\varepsilon)(\varepsilon - \mu)^m \left(-\frac{\partial f(\varepsilon, \mu)}{\partial \varepsilon} \right) \quad (9)$$

For ballistic phononic transport, the calculation of phonon transmission is similar to electron transmission. The difference is that electron transmission is calculated from hamiltonian matrix H but phonon transmission is calculated from dynamic matrix D .

$$T_p(\omega) = \text{Tr}(G_p^r \Gamma_L G_p^a \Gamma_R) \quad (10)$$

$$\Gamma_L = i(\Sigma_L^r - \Sigma_L^a), \Gamma_R = i(\Sigma_R^r - \Sigma_R^a) \quad (11)$$

$$G_p^r = [\omega^2 - D - \Sigma_L^r - \Sigma_R^r]^{-1} \quad (12)$$

From above equations, the phonon transmission function $T_p(\omega)$ at frequency ω is calculated. And the phonon thermal conductivity can be written as^{2,25}

$$\kappa_p(T) = \frac{\hbar^2}{2\pi K_B T^2 l} \int_0^{\infty} d\omega \omega^2 T_p(\omega) \frac{e^{\hbar\omega/k_B T}}{(e^{\hbar\omega/k_B T} - 1)^2} \quad (13)$$

III. RESULTS AND DISCUSSION

To obtain the thermoelectric properties of the InP₃ monolayer, we first study its electronic transport properties. The electronic band structure is given in Fig. 1(c), the top of valance bands (E_{HOMO}) is -0.365 eV, the bottom of conduction bands (E_{LUMO}) is 0.365 eV. The work of Miao *et al* has pointed out that the top valance bands are mainly contributed by the P's 3*p* and In's 5*p* orbits. They have also related such dispersion of valance band with the Mexican-hat-like shape to the excellent magnetic, electrical and optical properties in the InP₃ monolayer¹⁹. Here, we focus on the thermoelectric property. The characteristic of band structure, especially for the valance bands close to the Fermi energy, benefits largely to the high power factor of the InP₃ monolayer. There are several bands including both heavy-hole and light-hole bands located at the Γ point near Fermi energy. The light bands contribute to the high mobility. And the heavy bands indicate the large effective masses, which leads to a high Seebeck coefficient since the S is proportional to the effective mass. Additionally, there are several heavy-hole bands, with similar energy value as those at Γ , at M and K points, which exhibits converged characteristic and multi-valley transport in material. On the other hand, the top valance bands close to the Fermi energy ($\mu = 0$) are very flat and intensive, as compared to the conduction bands. This corresponds to a high density of states and will lead to a large transmission coefficient for such valance bands.

Fig. 1(d) gives the electronic transmission spectrum along the zigzag direction. A bandgap can also be observed, and moreover the transmission coefficient for the valance bands (below the Fermi energy $\mu < 0$) is indeed evidently larger than that for the conduction bands ($\mu > 0$), which is consistent with the feature of the band structure.

The electronic conductivity σ vanishes for chemical potential in the band gap at zero temperature. As the temperature is sufficiently high, transport is mediated by activated electrons and/or holes. Therefore, the nonzero conductivity appears inside the bandgap due to the finite temperature. The electronic conductivity σ as a function of the chemical potential μ is shown in Fig. 2(a) at 200 K, 300 K and 350 K, respectively. It shows that the σ below the Fermi energy is evidently larger than above the Fermi energy, and shows a few peaks which correspond to those of the transmission spectrum (Fig. 1(d)). Figure 2(b) gives the Seebeck effect S as a function of the chemical potential at temperatures of 200 K, 300 K, and 350 K, respectively. It can be seen that there are two peaks located below and above the Fermi energy, respectively, and inside the bandgap. Above (below) the Fermi energy, the S is negative (positive) and its absolute value increases sharply and monotonously until a maxima is reached. For a positive (negative) chemical potential $\mu > 0$ ($\mu < 0$), the major charge carriers are electrons (holes), which flow from the left to the right at

a positive temperature difference (ΔT) between the left and right. Therefore, the thermocurrent flows from the right to the left, and thus a positive (negative) voltage is needed to block the current, and hence the S is negative (positive) according to its definition. In addition, the maxima of S increases with the decreasing temperature, showing a sensitive dependence on the temperature. The appearance of the maxima of the S can be ascribed to the relationship of the $S \propto L_1/L_0$, according to Eq.7. Due to the factor $E - \mu$ in L_1 , this function decreases with decreasing temperature faster than L_0 does. Therefore, the interplay of the T dependence on the L_0 and L_1 functions leads to the maxima of the S .

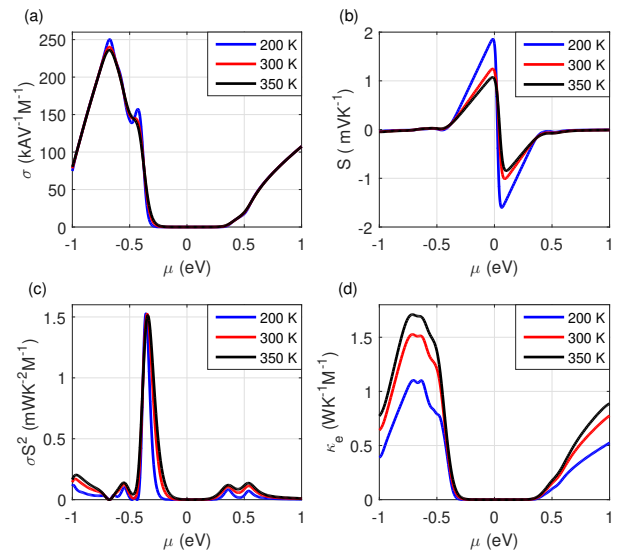


FIG. 2: (a) Electronic conductivity σ , (b) Seebeck coefficient S , (c) power factor σS^2 , and (d) the thermal conductivity of electrons κ_e as a function of chemical potential μ , respectively.

The power factor σS^2 at these temperatures is shown in Fig. 2(c). A sharp peak of power factor is located at $\mu - E_{\text{HOMO}} = 0.018$ eV when temperature is 300 K. Fig. 2(d) gives the thermal conductivity of electrons κ_e as a function of chemical potential μ , which increases with the increasing temperature.

Having known the electronic transport properties of the InP₃ monolayer, we now investigate its thermal transport properties. The phonon dispersion curves are shown in Fig. 3(a), which is symmetrical with respect to the Γ point for the $\Gamma \rightarrow \text{K}$ and $\Gamma \rightarrow \text{M}$ directions, suggesting an approximately isotropic thermal properties between the zigzag and armchair directions. There are twenty four curves in the phonon band structure that are contributed by the vibration modes of the two In atoms and six P atoms in the primitive cell. The three lowest curves correspond to the three acoustic branches, that is, the z-direction acoustic (ZA) mode, in-plane transverse acoustic (TA) mode, and longitudinal acoustic (LA) mode. These three types of acoustic phonon modes have the highest group velocities among all phonon modes, thus

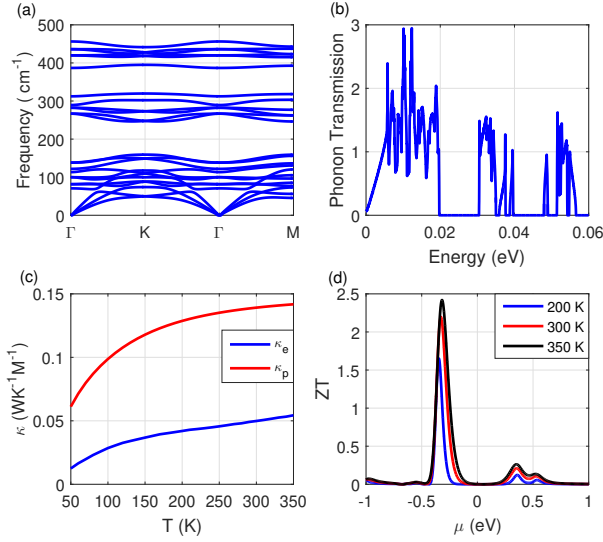


FIG. 3: (a) Phonon spectrum of the InP₃ monolayer, and (b) the corresponding phonon transmission spectrum. (c) The phononic thermal conductivity κ_p , and electronic thermal conductivity κ_e . (d) The figure of merit ZT as a function of chemical energy.

they contribute most importantly to the thermal conductivity. The group velocity can be calculated by $\partial\omega/\partial k$, which are 1.04 kms⁻¹, 0.72 kms⁻¹ and 0.56 kms⁻¹ for the LA, TA, and ZA phonon modes, respectively. These group velocities are about one order lower than those of the monolayer black phosphorous²⁶. On the other hand, the whole dispersions of phonons are very flat and exhibit highly localized properties as shown in Fig. 3(a), which demonstrates the low group velocities for most band branches. Note that a low phonon group velocity will lead to weak thermal transport capability, which means a lower thermal conductivity, and thus a higher ZT is to be expected.

The phonon transport spectrum is shown in Fig. 3(b). It shows that the thermal transmission is larger for the modes with energy lower than 0.02 eV. Importantly, these low energy phonon modes will give a major contribution to the phonon thermal conductivity κ_p for the temperature below 300 K. The dependence of the κ_p on the temperature is shown in Fig. 3(c). The κ_p shows a monotonous increase with increasing temperature. In comparison, the thermal conductivity contributed from electrons (κ_e) is also shown in the figure. The κ_p is approximately 2.8 times larger than the κ_e at 300 K, indicating that the phonon thermal conductivity has a larger influence on the thermoelectric properties. Figure 3(d) gives the figure of merit ZT at 200 K, 300 K and 350 K, as a function of chemical potential. We found that there are several ZT peaks located around the Fermi energy, and the maximum ZT is located at $\mu - E_{\text{HOMO}} = 0.037$ eV with a large $ZT = 2.2$ at 300 K. This should be attributed to the large peak of the power factor σS^2 at this chemical energy. Moreover, the maximum ZT increases

with the increasing temperature as shown in Fig. 4(a), with the peak location shifting closer to the Fermi energy. In addition, we found that InP₃ monolayer has an isotropic thermoelectricity properties, as it has an approximately same ZT along both zigzag and armchair directions, as shown in Fig. 4.

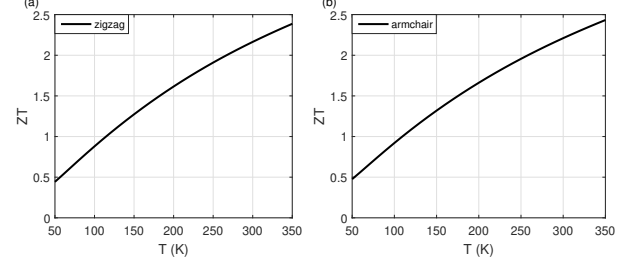


FIG. 4: The variation of the figure of merit ZT with temperature for the zigzag and armchair directions, respectively.

The large ZT (2.2) of InP₃ monolayer at room temperature outperforms that of other 2D materials ever reported, and is rather competitive in commercial applications. We found the phononic thermal conductivity of the InP₃ monolayer is 0.14 W(mK)⁻¹, which is relatively less than several other 2D materials at 300K, such as silicene, germanene and SnSe.^{27,28} For example, the thermal conductivity of the single-layered SnSe sheet is 2.57 W(mK)⁻¹.²⁸ Thus the relatively lower thermal conductivity of the InP₃ monolayer takes an important responsibility to its large ZT .

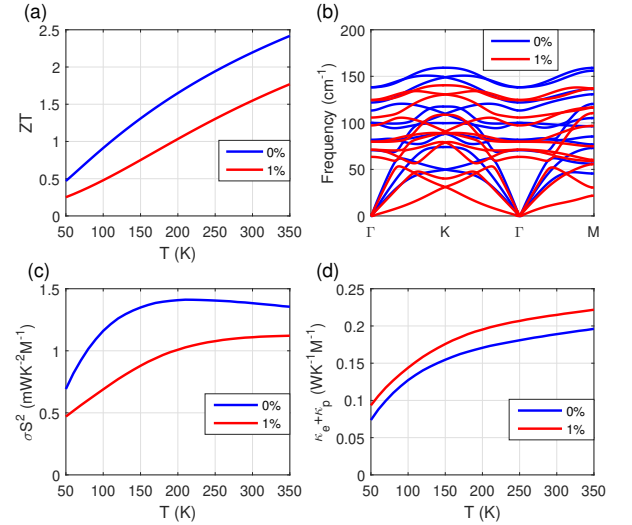


FIG. 5: (a) the ZT , (b) the phonon bands, (c) the power factor, and (d) the thermal conductivity ($\kappa_e + \kappa_p$) for the mechanic extension of 0% and 1%, respectively.

We now consider the influence of the mechanic strain on the figure of merit ZT . Under the compression, the system is not stable and large imaginary frequency appears, while it is stable under the extension. In Fig. 5(a),

we show the ZT of the InP_3 monolayer for the extension ratio of 0% and 1%. It shows clearly that the ZT drop obviously with the extension, which is 1.55 at the 300 K for the 1% mechanic extension strain. However, the ZT under mechanic extension strain is still considerably large, as it is greater than 1.5. Fig. 5(b) shows the phonon bands for 0% and 1%, respectively. From the results, we can find that the phonon frequency is decreased under the mechanic extension throughout. The decrease of the ZT under the mechanical extension can be understood from the variation in the thermal conductivity and the power factor σS^2 . Fig. 5(c) shows that under the 1% mechanic extension strain, the power factor decreases significantly, as compared to the case without strain, which will decrease the ZT . On the other hand, thermal conductivity increases a little under strain (Fig. 5(d)), which will also decrease the ZT . These two effects lead to decrease the ZT finally, as the effect in the power factor is more severely than that of the thermal conductivity.

It should be noted that the transport of the thermal properties is calculated within the ballistic transport region. It means that other factors like phonon-phonon scattering effects and electron-phonon scattering effects which are important in higher temperatures are not considered. These factors can be safely eliminated below the Debye temperature. We estimated that the Debye temperature is about 380 K, which is obtained by fitting the Debye formula²⁹,

$$C_v = 9Nk_B \left(\frac{T}{\Theta_D}\right)^3 \int_0^{\Theta_D/T} \frac{x^4 e^x dx}{(e^x - 1)^2}, \quad (14)$$

where $x = \hbar\omega/k_B T$. The isometric heat capacity C_v can be obtained by

$$C_v = \sum_{n,\mathbf{q}} k_B \left(\frac{\hbar\omega_n(\mathbf{q})}{k_B T}\right)^2 \frac{e^{\hbar\omega_n(\mathbf{q})/k_B T}}{(e^{\hbar\omega_n(\mathbf{q})/k_B T} - 1)^2}, \quad (15)$$

where \hbar is the reduced Planck constant, k_B is Boltzmann constant, T is the temperature, and $\omega_n(\mathbf{q})$ is the phonon frequency of the n th branch with wave vector \mathbf{q} . We could solve Eq.(14) numerically, and get the temperature-

dependent Debye temperature. We determine the Debye temperature, which is the value at the temperature point where the heat capacity is equal to the half of Dulong and Petit value. Above the Debye temperature, all the phonon modes are activated, and the phonon-phonon scattering would dominate in determining the behavior of temperature-dependent thermal conductivity, which would decrease with temperature according to the $1/T$ relation. More importantly, due to the 2D property of present system of InP_3 , the phonon-surface scattering in decreasing the heat conductivity outweighs the importance of phonon-phonon scattering, which is just like that in many film systems³⁰. Then the anharmonic effects is of limited importance, and the ballistic transport is expected to be good in describing the behavior of heat conductivity of the InP_3 monolayer at lower temperature. Therefore, the high ZT of 2.2 at 300 K for the InP_3 monolayer is reliable in this work.

IV. CONCLUSIONS

In summary, we have studied the intrinsic thermoelectrical properties of the InP_3 monolayer using the quantum transport calculations within the ballistic transport region. Our calculation shows that there are the converged valance band structures near the Fermi energy, which benefits the high power factor in the InP_3 monolayer. More importantly, the low group velocities of phonons leads to the low thermal conductivity. And it leads to high thermoelectric performance of the InP_3 monolayer. Moreover, the ZT can be greater than 1.5, even if a certain mechanic extension ($\leq 1\%$) is applied on the lattice. Our work gives an insight to searching high ZT materials at room-temperature.

V. ACKNOWLEDGEMENTS

This work was supported by the National Natural Science Foundation of China under Grants Nos. 11404348, 11504395 and 51871156.

* Electronic address: yqxie@shnu.edu.cn

† Electronic address: hzshao@nimte.ac.cn

‡ Electronic address: ybhu@mail.sitp.ac.cn

¹ D. M. Rowe, editor. *CRC Handbook of Thermoelectrics*. CRC Press, Boca Raton, FL, 1995.

² T. Markussen, Antti-Pekka Jauho, and Mads Brandbyge. Spintronics: Fundamentals and applications. *Phys. Rev. Lett.*, 103:055502, 2009.

³ Li-Dong Zhao, Shih-Han Lo, Yongsheng Zhang, Hui Sun, Gangjian Tan, Ctirad Uher, C. Wolverton, Vinayak P. Dravid, and Mercouri G. Kanatzidis. Ultralow thermal conductivity and high thermoelectric figure of merit in snse crystals. *Nature*, 508:373, 2014.

⁴ Cheng Chang, Minghui Wu, Dongsheng He, Yanling Pei, Chao-Feng Wu, Xuefeng Wu, Hulei Yu, Fangyuan Zhu, Kedong Wang, Yue Chen, Li Huang, Jing-Feng Li, Jiaqing He, and Li-Dong Zhao. 3d charge and 2d phonon transports leading to high out-of-plane zt in n-type snse crystals. *Science*, 360:778, 2018.

⁵ A. I. Hochbaum, R. Chen, R. D. Delgado, W. Liang, E. C. Garnett, M. Najarian, A. Majumdar, and P. Yang. Enhanced thermoelectric performance of rough silicon nanowires. *Nature*, 451:163, 2008.

⁶ Wen Huang, Haixia Da, and Gengchiao Liang. Thermoelectric performance of mx2 monolayers. *J. Appl. Phys.*, 113:104304, 2013.

- ⁷ Darshana Wickramaratne, Ferdows Zahid, and Roger K. Lake. Electronic and thermoelectric properties of few-layer transition metal dichalcogenides. *J. Chem. Phys.*, 140:124710, 2014.
- ⁸ Cem Sevik and Haldun Sevincli. Promising thermoelectric properties of phosphorenes. *Nanotechnology*, 27:355705, 2016.
- ⁹ K. Zborecki, M. Wierzbicki, J. Barnas, and R. Swirkowicz. Thermoelectric effects in silicene nanoribbons. *Phys. Rev. B*, 88:115404, 2013.
- ¹⁰ K. Yang, S. Cahangirov, A. Cantarero, A. Rubio, and R. D’Agosta. Thermoelectric properties of atomically thin silicene and germanene nanostructures. *Phys. Rev. B*, 89:125403, 2014.
- ¹¹ Leonardo Medrano Sandomas, David Teich, Rafael Gutierrez, Tommy Lorenz, Alessandro Pecchia, Gotthard Seifert, and Gianaurelio Cuniberti. Anisotropic thermoelectric response in two-dimensional puckered structures. *J. Phys. Chem. C*, 120:18841, 2016.
- ¹² Kedar Hippalgaonkar, Ying Wang, Yu Ye, Diana Y. Qiu, Hanyu Zhu, Yuan Wang, Joel Moore, Steven G. Louie, and Xiang Zhang. High thermoelectric power factor in two-dimensional crystals of mos2. *Phys. Rev. B*, 95:115407, 2017.
- ¹³ Zi-Yu Hu, Kai-Yue Li, Yong Lu, Yan Huang, and Xiao-Hong Shao. High thermoelectric performances of monolayer snse allotropes. *Nanoscale*, 9:16093, 2017.
- ¹⁴ X. M. Wang, D. C. Mo, and S. S. Lu. On the thermoelectric transport properties of graphyne by the first-principles method. *J. Chem. Phys.*, 138:204704, 2013.
- ¹⁵ Kai-Xuan Chen, Shu-Shen Lyu, Xiao-Ming Wang, Yuan-Xiang Fu, Yi Heng, and Dong-Chuan Mo. Excellent thermoelectric performance predicted in two-dimensional buckled antimonene: A first-principles study. *J. Phys. Chem. C*, 121:13035, 2017.
- ¹⁶ Gang Zhang and Yong-Wei Zhang. Thermoelectric properties of two-dimensional transition metal dichalcogenides. *J. Mat. Chem. C*, 5:7684, 2017.
- ¹⁷ Daniel Olaya, Mikel Hurtado-Morales, Daniel Gomez, Octavio Alejandro Castaneda-Urbe, Zhen-Yu Juang, and Yenny Hernandez. Large thermoelectric figure of merit in graphene layered devices at low temperature. *2D material*, 5:011004, 2018.
- ¹⁸ S. Sharma, S. Kumar, and U. Schwingenschlogl. Arsenene and antimonene: Two-dimensional materials with high thermoelectric figures of merit. *Phys. Rev. Applied*, 8:044013, 2017.
- ¹⁹ Naihua Miao, Bin Xu, Nicholas C. Bristowe, Jian Zhou, and Zhimei Sun. Tunable magnetism and extraordinary sunlight absorbance in indium triphosphide monolayer. *J. Am. Chem. Soc.*, 139:11125, 2017.
- ²⁰ Jeremy Taylor, Hong Guo, and Jian Wang. *Ab initio* modeling of quantum transport properties of molecular electronic devices. *Phys. Rev. B*, 63:245407, 2001.
- ²¹ G. Kresse and J. Furthmüller. Efficient iterative schemes for *ab initio* total-energy calculations using a plane-wave basis set. *Phys. Rev. B*, 54:11169–11186, 1996.
- ²² P. E. Blochl. Projector augmented-wave method. *Phys. Rev. B*, 50:17953, 1994.
- ²³ J. P. Perdew, J. A. Chevary, S. H. Vosko, K. A. Jackson, M. R. Pederson, D. J. Singh, and C. Fiolhais. Atoms, molecules, solids, and surfaces: Applications of the generalized gradient approximation for exchange and correlation. *Phys. Rev. B*, 46:6671, 1992.
- ²⁴ For details of nanodcal software package, please refer to: <http://www.hzwtech.com>.
- ²⁵ Takahiro Yamamoto and Kazuyuki Watanabe. Nonequilibrium green’s function approach to phonon transport in defective carbon nanotubes. *Phys. Rev. Lett.*, 96:255503, 2006.
- ²⁶ Jin-Wu Jiang. Thermal conduction in single-layer black phosphorus: highly anisotropic. *Nanotechnology*, 26:055701, 2015.
- ²⁷ Y. D. Kuang, L. Lindsay, S. Q. Shi, , and G. P. Zheng. Tensile strains give rise to strong size effects for thermal conductivities of silicene, germanene and stanene. *Nanoscale*, 8:3760, 2016.
- ²⁸ Fancy Qian Wang, Shunhong Zhang, Jiabing Yuc, and Qian Wang. Thermoelectric properties of single-layered snse sheet. *Nanoscale*, 7:15962, 2015.
- ²⁹ Hezhu Shao, Xiaojian Tan, Jun Jiang, and Haochuan Jiang. First-principles study on the elastic properties of cu₂gese₃. *EPL (Europhysics Letters)*, 113:26001, 2016.
- ³⁰ T. Tritt, editor. *Thermal conductivity: theory, properties, and applications*. Kluwer Academic / Plenum Publishers, New York, Boston, Dordrecht, London, Moscow, 2003.